Scalable production of multifunctional bio-based polyamide 11/graphene nanocomposites by melt extrusion processes via masterbatch approach

B. Rashmi, K. Prashantha, M.-F. Lacrampe, P. Krawczak

Scalable Production of Multifunctional Bio-Based Polyamide 11/Graphene Nanocomposites by Melt Extrusion Processes Via Masterbatch Approach

B. J. RASHMI, K. PRASHANTHA, M.-F. LACRAMPE, P. KRAWCZAK

Mines Douai, Department of Polymers and Composites Technology & Mechanical Engineering, 941 rue Charles Bourseul, CS 10838, F-59508 Douai, France

Correspondence to: Kalappa Prashantha, e-mail: kalappa.prashantha@mines-douai.fr.

Received: March 16, 2016
Accepted: July 30, 2016

ABSTRACT: Bio-based polyamide 11 (PA11)–graphene nanoplatelets (GNP) nanocomposites with different filler concentrations were prepared by melt extrusion using a masterbatch dilution process. Graphene platelets are uniformly distributed into the polymer matrix as revealed by scanning electron microscopy. The incorporation of graphene significantly improves the electrical conductivity and dielectric constant of PA11. GNPs favors the matrix crystallization; crystallization temperature and degree of crystallinity of the nanocomposites tend to increase with increase in graphene loading. Tensile properties (strength and modulus) are slightly improved by the incorporation of GNP into the PA11 matrix (up to +25% and +56%, respectively, for 5 wt% GNPs) at the expense of ductility (elongation at break divided by 5 for 5 wt% GNPs). © 2016 Wiley Periodicals, Inc. Adv Polym Technol 2018, 37, 21757; View this article online at wileyonlinelibrary.com. DOI 10.1002/adv.21757

KEY WORDS: Electrical properties, Graphene, Mechanical properties, Nanocomposites, Polyamide 11

Introduction

Polyamide 11 (PA11) is a bio-based polymer produced from renewable castor oil. Its versatility with many different properties such as relatively high thermal stability, very low moisture pick-up, excellent chemical resistance, and good mechanical properties makes it outstanding for outdoor applications, which requires high performances in extreme environment conditions. Graphene, a two-dimensional sheet composed of SP^2 carbon atoms arranged in a honeycomb structure, is fundamentally single layer of graphite, found in nature in the form of natural graphite flakes. Single-layer graphene is the strongest material (Young's modulus of 1 TPa and ultimate strength of 130 GPa) with a high thermal and electrical conductivity, extremely high surface area, and gas impermeability. It presents therefore a great potential for improving mechanical, electrical, thermal, and gas barrier properties of polymers.[1–7] Graphene, first produced in 1970 has thus drawn attention in the recent days as filler in conductive polymer nanocomposites.

However, despite the potential properties of graphene nanoplatelets (GNPs), preparation methods to integrate them in thermoplastics, such as in situ polymerization, solvent mixing, or melt mixing,[8] have low yield and high production costs[9] due to the large amount of solvents and/or energy required for the dispersion of nanofillers. Thus, there is a huge demand for a scalable and cost-effective fabrication technique of graphene-based nanocomposites. From an industrial point of view, melt compounding is the preferred technique as it is cost effective, environment friendly, and provides fast and continuous production.

Xu et al. reported preparation of graphene–polyamide 6 (PA6) nanocomposites by in situ ring-opening polymerization of caprolactam in the presence of graphene oxide (GO). By condensation reaction, the GO was reduced to graphene and effectively grafted by macromolecular chains of PA6. A good compatibility of GO with PA6 matrix was obtained as the modified graphene acted as great reinforcements to PA6 fibers due to enhanced interfacial interaction with the matrix. This might be the reason for the enhancement of tensile strength (increased by 2.1-fold) and Young's modulus (increased by 2.4-fold) of produced PA6–graphene nanocomposite fibers, even at very low content of graphene (0.1 wt%).[10] Similarly, Zheng et al. reported electrically conductive PA6 nanocomposites by in situ polymerization. Enhanced conductivity was achieved due to the exfoliated and dispersed graphene oxide (GO) nanosheets which were thermally reduced during the polymerization. In this case, the eclectic conductivity increased by more than 10 orders of magnitude when the GO critical contents increased from 0 to 0.41 wt%, the electrical threshold. No information was given concerning the effect of the addition of GO on the thermomechanical properties. Nevertheless, this simple in situ reduction and polymerization process

opened new way to fabricate graphene-based polymer nanocomposites cost effectively for a wide range of practical applications.[11] Liu et al. reported significant improvement in the tensile strength (from 299 to 425 MPa for neat matrix and nanocomposites containing 0.05 wt% graphene, respectively) of functionalized graphene–PA6 nanocomposite fibers, but also a slight reduction in the elongation at break (from 27.1% to 23.3%). No information was given concerning the electrical properties.[12] Jin et al. prepared functionalized graphene (FG)/PA11 and PA12 nanocomposites, and found that the vapor and gas barrier properties were improved by 49% and 47%, respectively, upon incorporation of a very small amount of the FG into the polymer matrices. The effect on the mechanical properties was limited (increase in Young's modulus and yield stress of 26% and 16%, respectively, and reduction in elongation at break of 18% in the case of PA12 containing 3 wt% of FG). The electrical properties of these nanocomposites have not been considered.[13] Mittal et al. has produced polymer–graphene nanocomposites based on high-density polyethylene (HDPE), low-density polyethylene (LDPE), polypropylene, polystyrene, and polycarbonate by melt processing to study the effect of filler amount on final properties of respective nanocomposites. They found that LDPE-based nanocomposites has shown significant enhancement in mechanical and rheological properties with increasing filler concentration and least enhancement was observed for PS nanocomposites which is due to processing conditions, polymer nature, and polarity compatibility between polymer and filler.[14] Graphene oxide-reinforced polyvinyl alcohol nanocomposites are produced to improve material properties. This enhancement is ascribed to strong interfacial interactions between the fillers and the matrix and homogeneous distribution of fillers.[15] One more approach to obtain materials with tuned properties is to blend immiscible polymers with low concentration nanofillers.[16,17] Finally, existing literature suggests that relatively little work has been published to date on the influence of graphene on the rheological and mechanical properties of PA11. This study aims to produce composites that possess high functional properties by cost-effective and scalable melt processing method.

It is well known that the dispersion of nanofillers in the polymer matrix influences the performance of nanocomposites. For other thermoplastic/nanofillers couples, better dispersion could be attained using a master batch dilution technique.[18–21] In masterbatch dilution technique, highly filled (around 15 wt%) masterbatch is to be prepared first and then diluted with the neat polymer to increase the filler dispersion. It is well-known fact that a better dispersion is due to the high shear stress acting on the masterbatch during the second dilution step. The high concentration of nanofiller in the masterbatch (usually 15 wt%) leading to high viscosity[22] associated with the longer residence time due to the second processing step is quite helpful to get a uniform dispersion of nanofiller in polymer matrix. Although a lot of studies have been carried out on graphene-filled polymer nanocomposites, existing literature suggests that relatively little work has been published to date on the influence of graphene on the electrical, dielectric, thermal, rheological, and mechanical properties of PA11. Therefore, in this study, PA11/graphene nanocomposites will be prepared by melt compounding via masterbatch dilution process. Effect of nanofillers on the morphology, rheological, electrical, thermal, and mechanical properties of the nanocomposites will be investigated.

Experimental

MATERIALS

Polyamide-11 is an injection molding grade (BMNO TLD, RilsanVR; Arkema, Colombes Cedex, France). Graphene nanoplatelets—grade 3—, have surface areas 600–750 $m^2\ g^{-1}$, 4–5 layers, an average thickness of 8 nm, and typical particle diameters of less than 2 μm (Cheap Tubes, Grafton, VT, USA). Before processing, PA11 pellets are dried under vacuum at 80°C for 8 h to remove moisture traces. Graphene nanoplatelets are used as received.

COMPOUNDING OF MASTERBATCHES

Masterbatch containing 15 wt% of graphene is prepared by dry-blending PA11 with the desired mass fractions of graphene, at room temperature. The PA11–graphene mixtures are then melt compounded in a twin-screw extruder (Haake Polylab OS; Thermoscientific, Waltham, MA, USA). The PA11 matrix is fed into the extruder barrel at feed port 1. To avoid the high stresses in the feeding zone, the GNP are fed separately in the melting zone where the matrix has already melted (Fig. 1). The temperature profile of the extruder is set at 220–235°C from feed zone to the die, respectively. The screw speed and feed rate are set at 60 rpm and 1 kg h^{-1}, respectively. Masterbatch pellets are then dried in vacuum oven at 80°C overnight to remove residual water content for further utilization.

PROCESSING OF NANOCOMPOSITES

The prepared PA11/graphene masterbatch is diluted to 0.5, 1, 3, and 5 wt% graphene-filled nanocomposites by melt compounding with neat PA11 granules in a twin-screw extruder (Haake Polylab OS; Thermoscientific) with abovementioned processing conditions with same screw profile (Fig. 1). The screw speed and feed rate are set at 75 rpm and 2 kg h^{-1}, respectively, based on our previous study.[21] Neat PA11 pellets are also extruded under the same conditions as a reference material. Standard test specimens for tensile, dynamic mechanical analysis, rheological, and dielectric measurements are molded using an injection-molding machine (Babyplast 6/10P, Chronoplast SL, Barcelona, Spain). The temperature profile ranges from 225 to 235°C and the mold temperature is maintained at 35°C with water-cooling system. All the materials are stored at 25°C and 50% relative humidity (RH) for 1 week before testing.

CHARACTERIZATION METHODS

The morphology of injection-molded cryofractured samples, previously coated with a thin gold layer (Polaron E5100 series II; Watford, Hertfordshire, UK), is observed under high vacuum with a Scanning Electron Microscope (SEM, S-4300SE/N; Hitachi, Tokyo, Japan) operating at 5 kV.

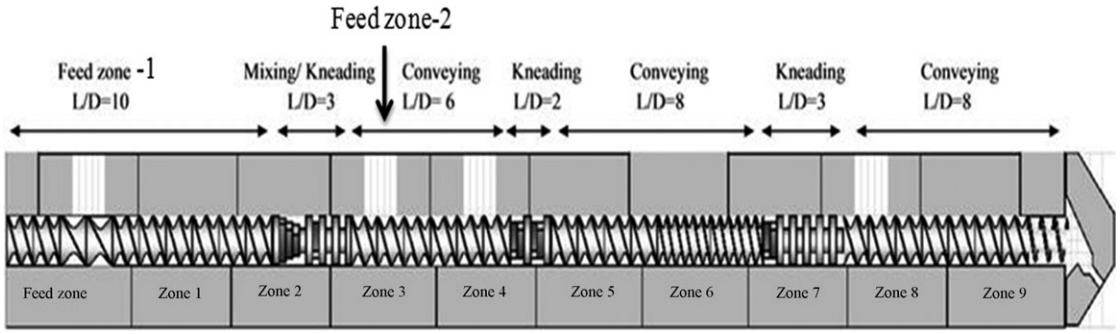

FIGURE 1. Extruder screw configuration showing feed ports for matrix (feed zone 1) and graphene (feed zone 2) with different mixing zones.

Thermal transitions of the materials are investigated by differential scanning calorimetry (DSC 7 Perkin-Elmer, Ithaca, NY, USA) under nitrogen flow (20 mL min^{-1}). Samples are crimple sealed in aluminum pans and heated from 30 to 220°C at a heating rate of 10°C min^{-1} (first heating scan), equilibrated at 220°C for 2 min, cooled at 10°C min^{-1} to 30°C, equilibrated at 30°C for 2 min, and then heated again to 220°C at 10°C min^{-1} (second heating scan). The first heating scan is performed to eliminate the sample's thermal history. The crystallization temperature (T_c), melting temperature (T_m), crystallization enthalpy (ΔH_c), melting enthalpy (ΔH_m), and degree of crystallinity, χ_c, are determined.

Oscillatory shear measurements are performed using an advanced rheometric system (Haake Mars III; ThermoScientific, Karlsruhe, Germany). Samples are equilibrated at 220°C for 10 min before testing. The measurements are performed at 220°C, under nitrogen atmosphere using plate and plate geometry (diameter: 35 mm and gap: 2 mm) with frequency sweep of 0.1–100 rad s^{-1}.

The viscoelastic behavior is studied in tension by dynamic mechanical analysis (DMA+150; MetraviB, ACOEM-Metravib, Limonest Cedex, France) on rectangular DMA specimens (nominal dimensions, $4 \pm 0.2 \times 10 \pm 0.5 \times 30$ mm^3) cut from injection-molded impact bar samples. Dynamic strain sweep is first performed to determine the linear viscoelastic domain of the materials. The tests are then performed at a strain amplitude of 0.02% and a frequency of 1 Hz. Data are collected from −50° to 120°C at a scanning rate of 3°C min^{-1}.

The surface electrical conductivity at room temperature is measured by the four-point probe method in van der Pauw configuration on 1 mm^2 plate (Using a Keithley 220 Programmable Current Source, a Keithley 2010 Multimeter as a voltmeter and a Keithley 705 Scanner equipped with a Keithley 7052 Matrix Card; Keithley Instruments, Beaverton, OR, USA). The dielectric characteristics of the materials are measured at 1000 Hz by using an impedance bridge (HP Agilent 4284A LCR meter; Agilent Technologies, Santa Clara, CA, USA). The accuracy of the dielectric measurement is confirmed by measuring the permittivity and tan δ of a standard polytetrafluoroethylene sample provided by the manufacturers. For each filler concentration, at least five samples are tested. All the measurements are performed at 25°C and 50% RH.

The mechanical properties are evaluated from injection-molded specimens. Tensile strength and elongation at break are measured at a crosshead rate of 3 mm min^{-1} and Young's modulus at 1 mm min^{-1}, using a tensile machine (Lloyd LR 50K, Largo, FL, USA) equipped with an extensometer at 25°C and 50% RH according to ISO 527 standard. At least five specimens of each composition are tested.

Results and Discussion

MORPHOLOGY

The homogeneous dispersion of fillers in the polymer matrix is one of the most important criteria to achieve optimal properties of nanocomposites. In case of GNPs, additional interplanar π–π interactions make it even more challenging to disperse them in the polymer matrices. Moreover, their hydrophobic nature is not favorable to their dispersion within the hydrophilic PA11 matrix. Nevertheless, Figs. 2a–2c show that GNPs are well dispersed in the PA11 matrix after dilution process, up to a GNPs concentration of 3 wt%. GNP's high aspect ratio and its relatively high population density facilitated it to form an interconnected filler network throughout the PA11 matrix during the masterbatch fabrication. The high shear forces induced during melt compounding in the extruder helped in breaking the agglomerates. However, at higher GNP concentration there is a high chance of re-agglomeration in the composites. As seen in Fig. 2d (at 5 wt%) there are GNP agglomerates in the matrix which could not be avoided during processing and few aggregates can be seen in nanocomposites bearing 5 wt% GNPs. The typical sizes of the agglomerates are in the range of 5 μm or smaller. Nilsson et al.[4] observed that solid-state mixed materials contain a significantly higher amount of laterally agglomerated (stacked) GNPs, whereas in our case, platelet-like structures are well dispersed in the matrix, probably because of low concentration of fillers. Jin et al.[13] observed that the graphene sheets were well dispersed and embedded in the polyamide matrices in nanocomposites prepared using a microextruder with low concentration of filler. Interestingly, in this study the use of a semi-industrial extruder and a masterbatch dilution process produces nanocomposites with a reasonably good dispersion at lower filler concentration.

CRYSTALLIZATION BEHAVIOR

DSC was employed to investigate the crystallization behavior of the PA11. The degree of crystallinity, χ_c, was calculated using Eq. (1):

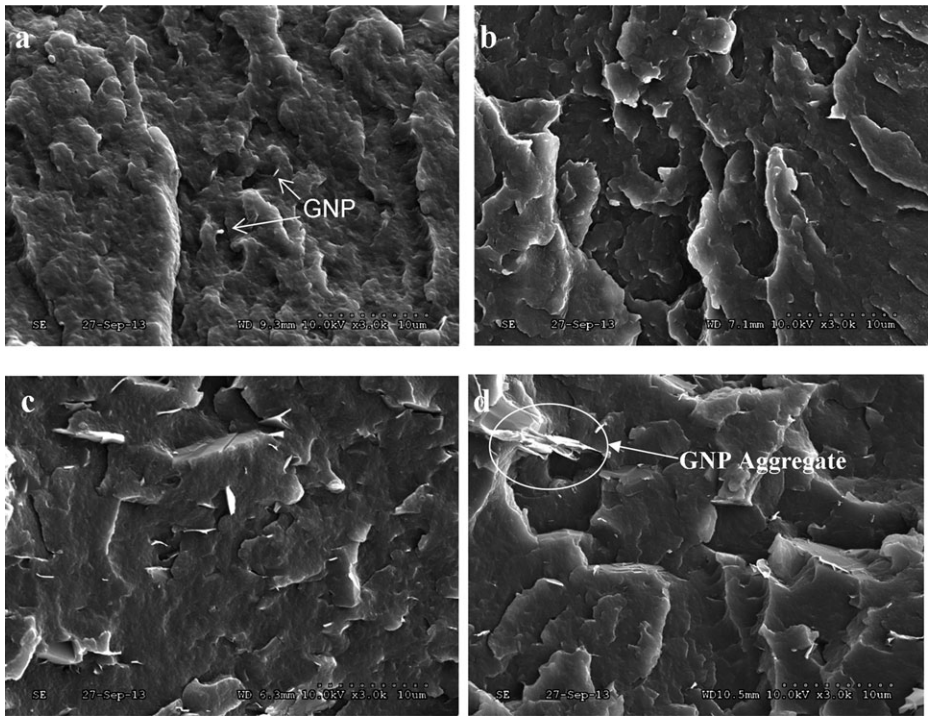

FIGURE 2. SEM images of polyamide 11 (PA11)/graphene nanoplatelet (GNP) systems (a) 0.5 wt% GNP, (b) 1 wt% GNP, (c) 3 wt% GNP, and (d) 5 wt% GNP.

$$\chi_c = \frac{\Delta H_m}{\Delta H_m^0 (1 - w_t)} \times 100 \quad (1)$$

where ΔH_m is the melting enthalpy, ΔH_m^0 the melting enthalpy for 100% crystalline sample (ΔH_c^0 = 206 J g^{-1}), and "w_t" the filler weight fraction in the nanocomposites. Figure 3 presents DSC thermograms of the PA11/GNP nanocomposites during the second heating (Fig. 3a) and cooling (Fig. 3b) at different filler concentrations.

Melting and crystallization temperatures (T_m, T_c), melting and crystallization enthalpies (ΔH_m, ΔH_c), and degree of crystallinity (χ_c) of PA11 nanocomposites as a function of GNP are shown in Table I. The addition of filler does not alter T_m, whereas χ_c increases from 15.5% to 22% with increase in GNP content. Also, a significant increase in T_c from 159 to 168°C is observed with increasing GNP content, meaning that GNPs in the PA11 matrix act as nucleating agents. This indicates that activation energy for crystallization is increased, due to the addition of GNP into PA11 matrix. Similar trends were reported by Jin et al.[13] for PA11/graphene nanocomposites.

RHEOLOGICAL PROPERTIES

Figure 4 shows the plot of storage shear modulus, G′ (Fig. 4a), and complex viscosity, η^* (Fig. 4b), as a function of angular frequency for neat PA11 and its nanocomposites prepared with GNP loadings of 0.5–5 wt%. PA11 shows a classical polymer melt behavior with G′ decreasing when lowering the frequency and a clear terminal zone in the low-frequency range. GNP-filled PA11 nanocomposites show an increase in G′ compared with neat PA11 and also as the graphene percentage increases. The reason for the increase in G′ might be the confinement of polymer chains within the graphene layers. Appearance of a pseudo-plateau in the low-frequency region for concentrations larger than 1 wt% is observed (Fig. 4a), i.e., elastic modulus and viscous modulus become nearly independent of frequency, which is consistent with the transition from liquid-like to pseudo-solid-like behavior of polymer melt with increasing GNP loading due to formation of polymer–graphene network.[20]

Comparing the present results with the literature, Nilsson et al.[4] observed that both viscosity and storage modulus were lower for the GNP-filled melts compared to the neat PP melt till 10 wt% GNP. Li and Zhong[9] reported a similar trend for 5 and 10 wt% GNP in PP melt. Kalaitzidou et al.[23] saw a slightly decreased viscosity at 2 wt% GNP and a moderate increase in viscosity for 6–20 wt% GNP in PP/GNP nanocomposites. The reduced viscosity compared to neat PP was referred to PP–GNP interlayer slipperiness due to a low surface friction. But, in this study both storage modulus and complex viscosity are higher than that of neat matrix indicating an absence of interlayer slipperiness. Also, the viscosity effect may thus also depend on the dispersion of GNP and preparation method.

VISCOELASTIC BEHAVIOR

Until glass transition temperature, the tensile storage modulus (E′) of PA11 also logically increases upon addition of GNP and all the more that GNP content increases. However, above the glass transition, E′ increase is no more significant (Fig. 5).

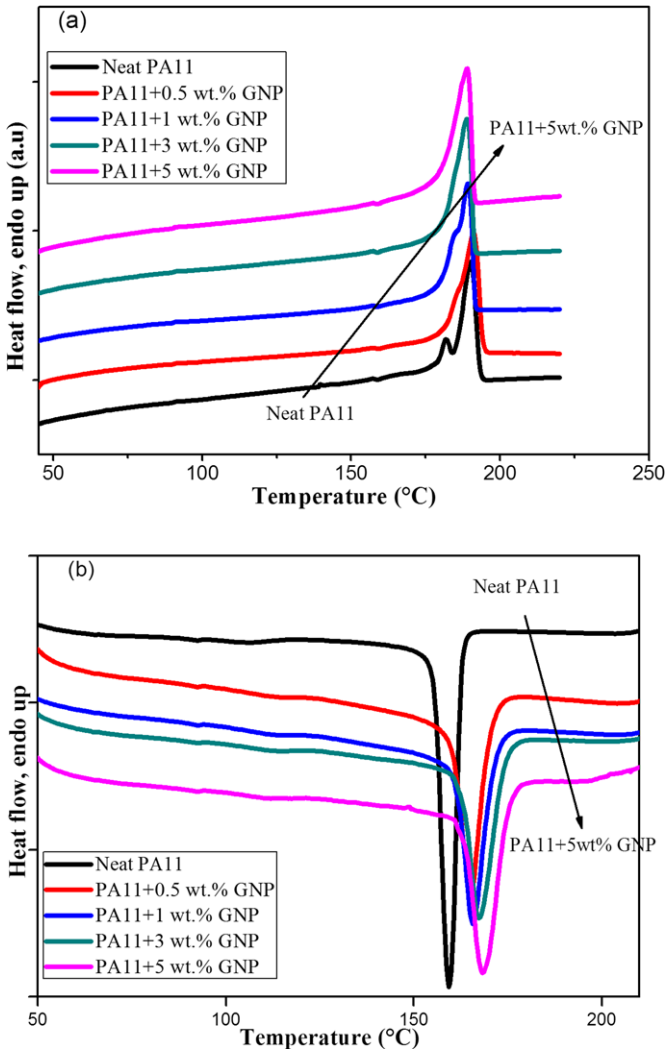

FIGURE 3. Differential scanning calorimetry (DSC) thermograms of polyamide 11 (PA11)/graphene nanoplatelets (GNPs) during second heating (a) and cooling (b).

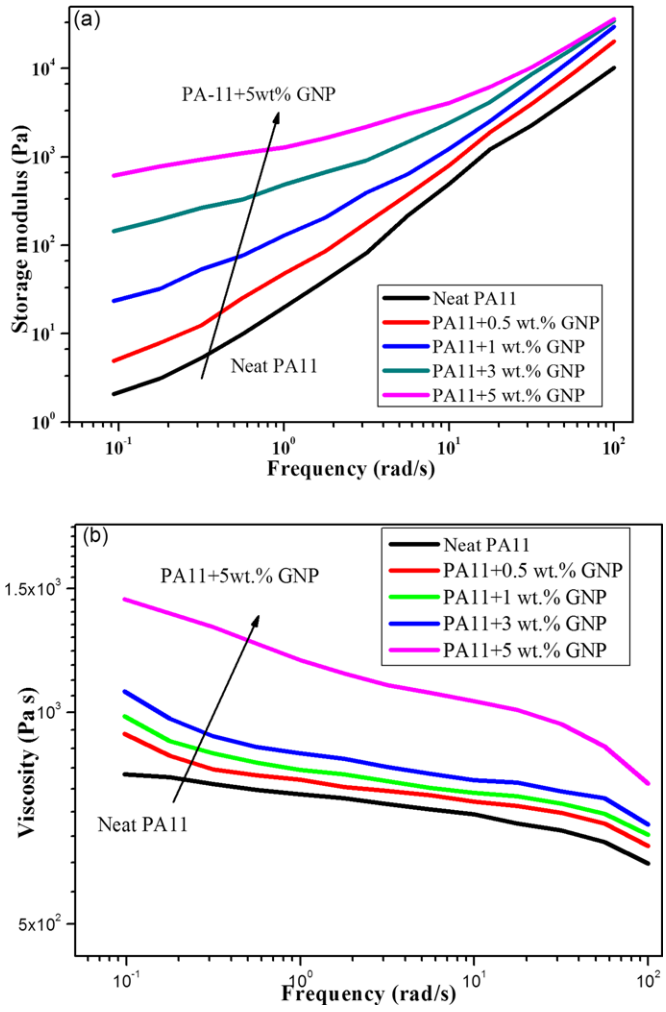

FIGURE 4. Storage shear modulus (G′) (a) and complex viscosity (η^*) (b) of polyamide 11 (PA11)/graphene nanoplatelet (GNP) nanocomposites with frequency sweep as a function of GNP content at 220°C.

TABLE I
Thermal Properties of polyamide 11 (PA11)/graphene nanoplatelet (GNP) Systems

Material	T_m (°C)	ΔH_m	T_c (°C)	ΔH_c	X_c (%)	T_g (°C)
Neat PA11	190	30	159	39	14.56	54.3
PA11+ 0.5 wt% GNP	190	34	163	22	16.58	56.8
PA11+ 1 wt% GNP	190	39	165	25	19.12	59.4
PA11+ 3 wt% GNP	189	40	167	26	20.01	60
PA11+ 5 wt% GNP	189	43	168	28	21.97	60.7

The tan δ peak is commonly referred to relaxations of the polymer related to the glass transition temperature (T_g) (see Table I). For neat PA11, the loss factor (tan δ) shows a peak at 54°C. This transition is shifted to the higher temperatures with increase in GNP content. T_g increases from 54.3 to 59.4°C at low filler content (i.e., at 0.5 and 1 wt%), and afterward

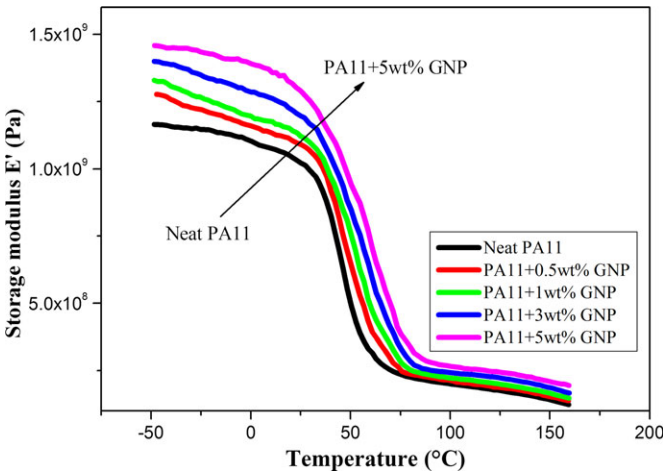

FIGURE 5. Storage tensile modulus E′ of polyamide 11 (PA11)/graphene nanoplatelet (GNP) nanocomposites with temperature sweep.

remains constant at higher concentration (>3 wt%). The increase in T_g from the pure PA11 system to the system filled with 1 wt% of GNPs is due to the fact that presence of the GNPs hinders the movement of the PA11 molecules and the interactions between PA11 and GNPs surfaces are expected to slow down the molecular dynamics of the composite system and therefore T_g of the nanocomposites has been shifted to higher temperatures.[24] At high filler loading (>3 wt%), since the free volume increases at higher filler content, the molecular mobility of the chains is only moderately slowed down by the interactions promoted between the GNP fillers and the PA11 matrix molecules leading to no change in the T_g.[25,26]

ELECTRIC AND DIELECTRIC PROPERTIES

Electrical conductivity of the nanocomposites is presented in Table II. Nanocomposite containing 0.5 wt% GNP shows conductivity of 2.2×10^{-6} S m^{-1} which indicates formation of good percolation network in the nanocomposites. Electrical conductivity increases slightly with growing filler concentration and the highest conductivity of 5.2×10^{-6} S m^{-1} is observed for 5 wt% GNP-filled nanocomposites. However, no visible electrical percolation is noticed in the studied sample due to the presence of saturated electrical tunneling network in the investigated composition range. Similarly, Lan et al.[17] observed conductivity of ~10^{-6} S m^{-1} for 0.5 wt% of reduced graphene oxide (RGO) in the thermoplastic polyurethane/polypropylene composites. Nilson et al. has measured electrical conductivity on samples prepared with two processing methods: solid-state mixing (SSM) and melt mixing (MM). The two methods affect significantly the electrical conductivity of extruded strands (7.9×10^{-6} S cm^{-1} for the SSM while the MM material shows 3.8×10^{-2} S cm^{-1} at 20 wt% GNP).[4]

Dielectric characterization can provide information on the molecular dynamics of polymer systems, monitoring the relaxation processes. It is determined by the ability of a material to polarize in response to the applied field. Owing to its frequency dependence, the permittivity of a material is often represented by the complex permittivity ε^* and is defined as

$$\varepsilon^* = \varepsilon' - \varepsilon''$$

where ε' is the real part or dielectric constant and ε'' is the imaginary part of the dielectric permittivity. The dielectric constant for a polymer depends on the polarizability of its molecules. High molecular polarizability leads to high ε^*. As a heterogeneous system, a composite has also its dielectric properties influenced by interfacial polarization, that is, charge buildup at the interfaces.

The real permittivity ε' increases with growing GNP concentration. This is ascribed to the polar characteristics of the fillers and thus to the increase in the number of charge carriers in the PA11 matrix. The increase in dielectric constant is attributed to the stronger dipole orientation polarization ability of PA11 caused by the disruption of hydrogen bonds of PA11 due to the homogeneous dispersion and compatibility of fillers in the PA11 matrix. Similar observations were made for grapheme/polyurethane nanocomposites.[27]

TABLE II
Electric and Dielectric Properties of polyamide 11 (PA11)/graphene nanoplatelet (GNP) Systems

Sample	Dielectric Constant at 1000 Hz	Conductivity (S m^{-1}) $\times 10^{-6}$
Neat PA11	3.0	–
PA11+ 0.5 wt% GNP	4.2	2.2 ± 0.01
PA11+ 1 wt% GNP	5.6	3.2 ± 0.03
PA11+ 3 wt% GNP	7.0	4.4 ± 0.07
PA11+ 5 wt% GNP	9.2	5.2 ± 0.09

MECHANICAL PROPERTIES

The typical tensile stress–strain curves of the neat PA11 and PA11/graphene nanocomposites are shown in Fig. 6. Table III presents the corresponding tensile properties. The incorporation of GNPs into PA11 has a significant influence on the mechanical behavior of nanocomposites. Addition of GNP to polymer matrix increases tensile strength (up to 25% for 5 wt% of GNP) and Young's modulus (up to 56% for 5 wt

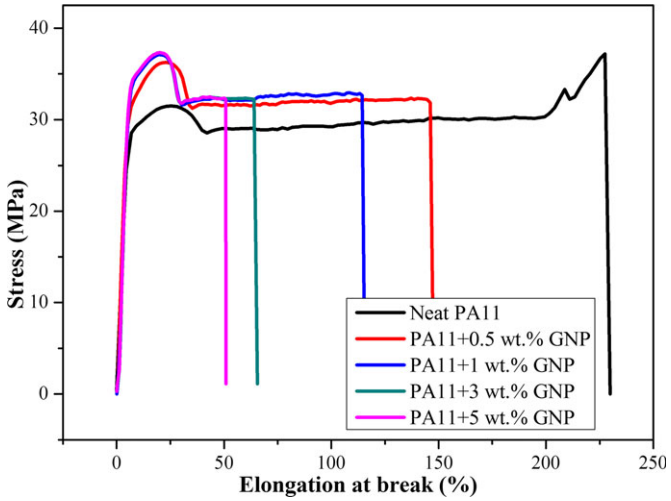

FIGURE 6. Tensile stress–strain curves of polyamide 11 (PA11)/graphene nanoplatelet (GNP) nanocomposites

TABLE III
Mechanical Properties of polyamide 11 (PA11)/graphene nanoplatelet (GNP) Systems

Sample	Young's Modulus (MPa)	Tensile Strength (MPa)	Elongation at Break (%)	Notched Impact Strength (kJ m^{-2})
Neat PA11	1126 ± 17.0	31.7 ± 1.1	249 ± 15.1	17.6 ± 0.4
PA11+ 0.5 wt% GNP	1524 ± 13.4	36.2 ± 0.2	137 ± 14.1	18.4 ± 0.3
PA11+ 1 wt% GNP	1630 ± 17.2	37.1 ± 0.2	88 ± 15.2	19.2 ± 0.2
PA11+ 3 wt% GNP	1689 ± 11.1	38.7 ± 0.4	64 ± 10.3	12.8 ± 0.1
PA11+ 5 wt% GNP	1756 ± 8.1	39.5 ± 0.5	50 ± 7.2	10.6 ± 0.1

% of GNP) but decreases drastically elongation at break of the nanocomposites (divided by 5 for 5 wt% of GNP). Importantly, all the nanocomposites retain a yield point and a small plastic deformation without showing any brittle behavior with increase in GNP concentration. Nanocomposites with 0.5 wt% GNP loading show 14% increase in tensile strength compared to that of the neat PA11. Further addition of GNP (1, 3, and 5 wt%) does not increase tensile strength significantly, probably because of the occurrence of GPN aggregation due to the van der Waals forces at the highest concentrations of GNP in

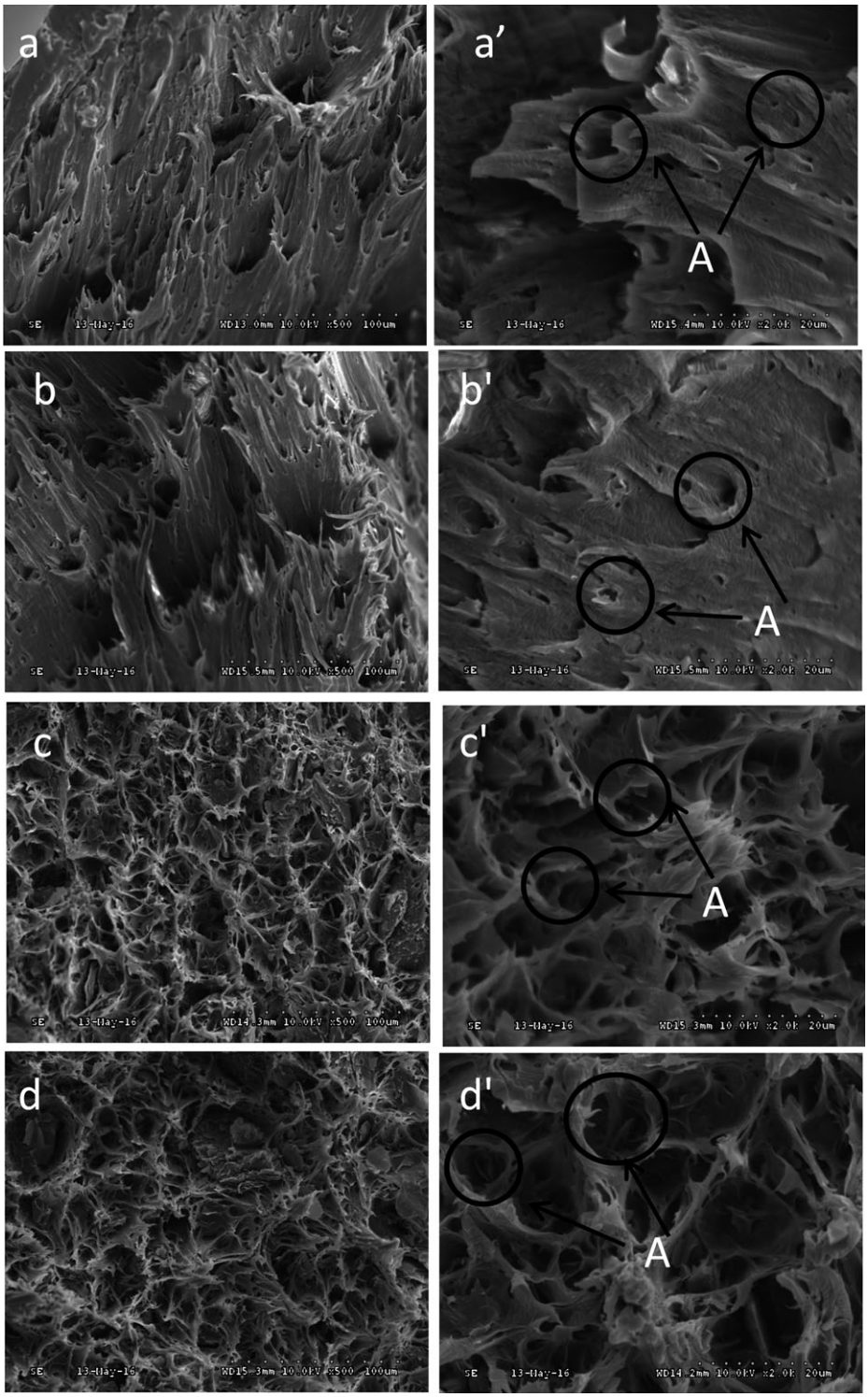

FIGURE 7. SEM images of tensile fractured polyamide 11 (PA11)/graphene nanoplatelet (GNP) samples at low and high magnification: (a and a′) 0.5 wt% GNP, (b and b′) 1 wt% GNP, (c and c′) 3 wt% GNP, and (d and d′) 5 wt% GNP, respectively.

the polymer matrix. Liu et al.[12] also observed increase in tensile strength at very low loading of graphene oxide (0.1 wt%) but a decrease at higher loading. The reason of this difference may be due to the different fillers used and also to the fillers orientation in fibers. The elongation at break of nanocomposites decreases with the increase in GNP loading. Neat polymer shows elongation at break of 249% ,whereas it is divided by ~2 for 0.5 wt% GNP loading, and by 5 for 5 wt% of GNP loading. Young's modulus increases by 35% with 0.5 wt% GNP loading compared to neat PA11, whereas further addition of GNP increases Young's modulus steadily. Generally, the mechanical properties of graphene polymer nanocomposites are strongly affected by the dispersion, aspect ratio, platelets/polymer interface, and the crystallinity of the polymer matrix. As we can see from Table I, increase in crystallinity of PA11 upon incorporation of graphene was observed and these crystalline properties of the nanocomposites may also contribute to the enhancement in the mechanical properties of the nancomposites at low filler loading.

To understand the fracture behavior, the fractured tensile specimens were characterized using SEM. Figure 7 shows representative SEM images of the fractured surfaces in both low and high magnification. There were many dimples (marked as A) on the fracture surfaces of the nanocomposites containing 0.5 and 1 wt% GNP and these nanocomposites showed a ductile fracture with plastic deformation and drawing of the matrix under tensile stress (Figs. 7a and 7b). Images taken at high magnification indicated that prominent deformation is of cavitational in nature (Figs. 7a′ and 7b′). Nanocomposites loaded with 3 and 5 wt% of GNP (Figs. 7c and 7d) clearly showed large dimples (marked as A) whose density and the size were much higher than 0.5 and 1 wt% GNP-filled nanocomposites, where presence of higher filler concentration rapidly led to microvoids, and thus crack initiated with large dimples (Figs. 7c′ and 7d′), which spoiled the plasticity of material.[28]

During impact testing all the specimens under study broke in an unstable manner. Table III shows the notched impact strength as a function of the GNP content. It can be seen that impact strength is slightly increased by the addition of 0.5 and 1 wt% of the GNP then decreases with increasing GNP content. Good dispersion of GNPs at lower concentration (0.5 and 1.0 wt%) marginally increase impact strength of PA11 matrix in comparison with neat matrix. This increase in toughness may be due to microplastic deformation with elongated crack patterns as shown in Figs. 8a and 8b. This elongated crack patterns possess higher crack growth resistance of the composites.[29] Nanocomposite filled with higher GNP concentrations (3 and 5 wt%) showed the decrease in notched impact strength in comparison with neat matrix. Reason for unfavorable impact properties is due to the presence of GNP agglomerates (marked as B) in PA11 at higher concentration (Figs. 8c and 8d).

Conclusions

The potential of using graphene nanoplatelets (GNP) as reinforcement for producing efficient polyamide 11 (PA11)-based nanocomposites by melt extrusion through masterbatch approach has been explored. Tensile strength, modulus,

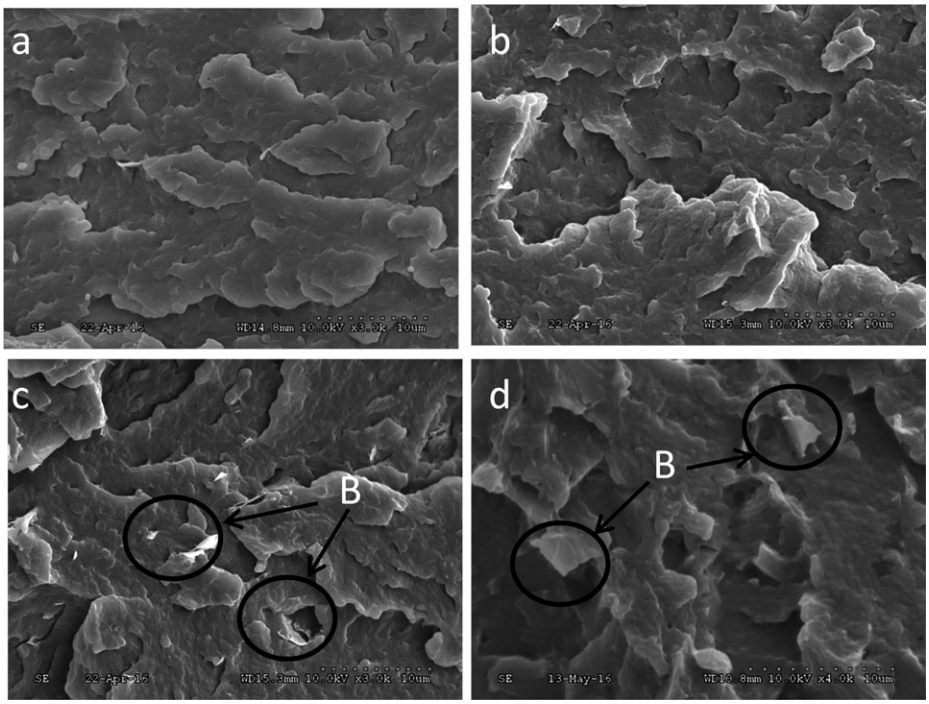

FIGURE 8. SEM images of impact fractured surfaces of polyamide 11 (PA11)/graphene nanoplatelet (GNP) samples: (a) 0.5 wt% GNP, (b) 1 wt% GNP, (c) 3 wt% GNP, and (d) 5 wt% GNP, respectively.

thermal, and electrical properties are improved by the incorporation of GNP into the PA11 matrix. Scanning electron microscopy confirmed that fillers are well dispersed in PA11 matrix. GNPs act as nucleating agents in the PA11 matrix, crystallization temperature and degree of crystallinity of the nanocomposites tending to increase with increase in graphene loading. Rheological study highlighted improvement in storage modulus and complex viscosity with increase in graphene weight percentage. Low-frequency plateau is observed at high graphene loading because of the pseudo-solid-like behavior of polymer melt. The dielectric constant and electrical conductivity of the nanocomposites also significantly increase with increase in GNP concentration, but without visible electrical percolation threshold. Besides, the tensile strength increases by ~14–25% and modulus by ~35–56%, for 0.5–5 wt% GNP, respectively, however, at the expense of the material ductility (elongation at break divided by 2–5, respectively). The widespread usage of carbon-based nanofillers in industrial workshops will cause emissions to the environment and result in an increase in human exposure to nanofillers. Upon exposure, these nanofillers may reach the lungs where they can exert serious toxicity by inflammatory and fibrotic reactions. Therefore, handling of carbon-based nanofillers in plastic parts manufacturing workshops is, however, often a key issue. Production of a GNP masterbatch in polyamide is an attractive alternative as it offers a dust-free processing method with lower health and safety risks compared to the bulk carbon nanofillers dispersion process and the solution casting methods used for the production of graphene-based polymer nanocomposites. Other benefits of using a masterbatch include elimination of dispersion difficulties and the need for formulation development, as well as an easier method for handling the material. Therefore, the masterbatch processing route is attractive for most polymer nanocomposites manufacturing industries where the carbon-based nanomaterials are bound in a polymer or are a polymer component, which makes them easier to handle.

Acknowledgments

The HYDRAX European project leading to these results has received funding from the Nord-Pas-de-Calais Region (France) under grant agreement no. 13000977 in the frame of the CrossTexNet Programme, an ERA-NET Plus financed by the European Union Seventh Framework Programme [(FP7/2007–2013)]. The authors also gratefully acknowledge the International Campus on Safety and Intermodality in Transportation (CISIT, France), the Nord-Pas-de-Calais Region (France), and the European Union (FEDER funds) for their contributions to funding the dynamic rheometer, the dynamic mechanical analysis equipment, and the extruder.

References

1. Fukushima, H. Graphite nanoreinforcements in polymer nanocomposites, PhD Thesis; Michigan State University: Michigan, 2003.
2. Lee, C.; Wei, X.; Kysar, J. W.; Hone, J. Science 2008, 321, 385–388.
3. Balandin, A. A.; Ghosh, S.; Bao, W.; Calizo, I.; Teweldebrhan, D.; Miao, F.; Lau, C. N. Nano Lett 2008, 8, 902–907.
4. Nilsson, E.; Oxfall, H.; Wandelt, W.; Rychwalski, R.; Hagström, B. J Appl Polym Sci 2013, 130(4), 2579–2587.
5. Du, X.; Skachko, I.; Barker, A.; Andrei, E. Y. Nat Nanotechnol 2008, 3, 491–495.
6. Bunch, J. S.; Verbridge, S. S.; Alden, J. S.; van der Zande, A. M.; Parpia, J. M.; Craighead, H. G.; McEuen, P. L. Nano Lett 2008, 8, 2458–2462.
7. Kim, H.; Abdala, A. A.; Macosko, C. W. Macromolecules 2010, 43, 6515–6530.
8. Kalaitzidou, K.; Fukushima, H.; Drzal, L. T. Compos Sci Technol 2007, 67, 2045–2051.
9. Li, B.; Zhong, W.-H. J Mater Sci 2011, 46, 5595–5614.
10. Xu, Z.; Gao, C. Macromolecules 2010, 43, 6716–6723.
11. Zheng, D.; Tang, G. S.; Zhang, H. B.; Yu, Z. Z.; Yavari, F.; Koratkar, N.; Lim, S. H.; Lee, M. W. Compos Sci Technol 2012, 72, 284–289.
12. Liu, H. H.; Peng, W.-W.; Hou, L.-C.; Wang, X.-C.; Zhang, X.-X. Compos Sci Technol 2013, 81, 61–68.
13. Jin, J.; Rafiq, R.; Gill, Y. Q.; Song, M. Eur Polym J 2013, 49, 2617–2626.
14. Mittal, V.; Chaudhry, A. U. Macromol Mater Eng 2015, 300, 510–521.
15. Kashyap, S.; Pratihar, S. K.; Behera, S. K.; Qi, X.; Yao, X.; Deng, S.; Zhou, T.; Fu, Q. J. Mater Chem A 2014, 2, 2240–2249.
16. Liebsche, M.; Blais, M.-O.; Pötschke, P.; Heinrich, G. Polymer 2013, 54, 5875–5882.
17. Lan, Y.; Liu, H.; Cao, X.; Zhao, S.; Dai, K.; Yan, X.; Zheng, G.; Liu, C.; Shen, C.; Guo, Z. Polymer 2016, 97, 11–19.
18. Soulestin, J.; Rashmi, B. J.; Bourbigot, S.; Lacrampe, M.-F.; Krawczak, P. Macromol Mater Eng 2012, 297, 444–454.
19. Prashantha, K.; Lacrampe, M.-F.; Krawczak, P. Express Polym Lett 2011, 5, 295–307.
20. Prashantha, K.; Soulestin, J.; Lacrampe, M.-F.; Krawczak, P. Compos Sci Technol 2009, 69, 1756–1763.
21. Prashantha, K.; Lacrampe, M.-F.; Krawczak, P. J Appl Polym Sci 2013, 130, 313–321.
22. Alig, I.; Pötschke, P.; Lellinger, D.; Skipa, T.; Pegel, S.; Kasaliwal, G. R.; Villmow, T. Polymer 2012, 53, 4–28.
23. Kalaitzidou, K.; Fukushima, H.; Drzal, L. T. Carbon 2007, 45, 1446–1452.
24. Ash, B. J.; Schadler, L. S.; Siegel, R. W. Mater Lett 2002, 55(1), 83–87.
25. Sushko, R.; Filimon, M.; Dannert, R.; Elens, P.; Sanctuary, R.; Baller, J. Nanotechnology 2014, 25, 425704.
26. Kosmidou, T. V.; Vatalis, A. S.; Delides, C. G.; Logakis, E.; Pissis, P., Papanicolaou, G. C. eXPRESS Polym Lett 2008, 2, 364–372.
27. Liu, S.; Tian, M.; Yan, B.; Yao, Y.; Zhang, L.; Nishi, T.; Ning, N. Polymer 2015, 56, 375–384.
28. Díez-Pascual, A. M.; Naffakh, M. Mater Chem Phys 2012, 135, 348–357.
29. Ryu, J.; Han, M. Compos Sci Technol 2014, 102, 169–175.